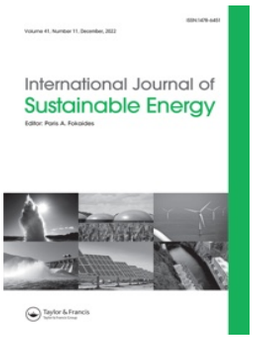

International Journal of Sustainable Energy

ISSN: 1478-6451 (Print) 1478-646X (Online) Journal homepage: www.tandfonline.com/journals/gsol20

Numerical investigation of building integrated solar thermal collectors under diverse conditions

Loucas Georgiou, Manolis Souliotis, Theodoros Leontiou, Jolanta Šadauskienė, Juozas Vaičiūnas, Spiros Papaefthimiou & Paris A. Fokaides

To cite this article: Loucas Georgiou, Manolis Souliotis, Theodoros Leontiou, Jolanta Šadauskienė, Juozas Vaičiūnas, Spiros Papaefthimiou & Paris A. Fokaides (2023) Numerical investigation of building integrated solar thermal collectors under diverse conditions, International Journal of Sustainable Energy, 42:1, 1042-1062, DOI: 10.1080/14786451.2023.2250868

To link to this article: https://doi.org/10.1080/14786451.2023.2250868

Published online: 29 Aug 2023.

INTERNATIONAL JOURNAL OF SUSTAINABLE ENERGY
2023, VOL. 42, NO. 1, 1042–1062
https://doi.org/10.1080/14786451.2023.2250868

Numerical investigation of building integrated solar thermal collectors under diverse conditions

Loucas Georgiou[a], Manolis Souliotis [b], Theodoros Leontiou[a], Jolanta Šadauskienė[c], Juozas Vaičiūnas[c], Spiros Papaefthimiou[d] and Paris A. Fokaides [a,c]

[a]School of Engineering, Frederick University, Nicosia, Cyprus; [b]Department of Chemical Engineering, University of Western Macedonia, Kozani, Greece; [c]Faculty of Civil Engineering and Architecture, Kaunas University of Technology Lithuania, Kaunas, Lithuania; [d]School of Production Engineering and Management, Technical University of Crete, Chania, Greece

ABSTRACT

The scope of this study is the investigation of the thermal performance of building-integrated solar flat collectors with a uniform and multiple riser structure. The effect of dynamic operating parameters such as the environmental temperature, solar radiation, the inclination angle and further model modifications to the fluid inlet, outlet and riser are studied. Numerical calculations were carried out using Finite Element (FE) analysis. Three-dimensional transient models were developed to calculate the thermal performance of the investigated objects. The study revealed increased efficiency for the multiple-riser configuration. Under all boundary conditions, the highest fluid temperatures occur in the south orientation during autumn and winter and in the west during spring and summer. The thermal assessment comparison between the roof installed and vertical solar collectors were performed, and the differences throughout the slope angles were distinguished. The results showed that a building-integrated solar system acted as a shield barrier, and provided heat to the building structure.

ARTICLE HISTORY
Received 13 December 2022
Accepted 22 July 2023

KEYWORDS
Solar collector; flat plate collector; building integrated solar thermal collector; transient heat transfer; finite elements

Nomenclature

e	Specific internal energy [J/kg]
H	Total energy of flowing fluid [J/kg]
h	Thermal enthalpy [J]
P	Pressure [Pa]
QH	Specific heat release or absorption per unit volume [J/(kg·K)]
q_i	Heat flux [w/m^2]
R	Gas constant [8.3145 J/mol·K]
T	Temperature [°C]
S_i	Mass-distributed external force per unit mass [N/kg]
u_i	Ith component of the carrier fluids velocity [-]
u_j	Jth component of the carrier fluids velocity [-]
u	Fluid velocity [m/s]
x_i	Ith component of the used coordinate system [-]
x_j	Jth component of the carrier fluids velocity [-]

CONTACT Manolis Souliotis msouliotis@uowm.gr

Greek Symbols

ε Turbulent dissipation [J/(kg·s)]
λ_i Eigenvalues of the thermal conductivity tensor
ρ Fluid density [kg/m^3]
τ_{ij} Viscous stress tensor [Pa]
τ_{ij}^R Reynolds stress tensor [Pa]

1. Introduction

The use of solar thermal collectors dates back to the '60s. In states of southern Europe and the Middle East like Cyprus, Greece, Italy, Spain and Israel, solar thermal collectors' use to produce domestic hot water is part of everyday life (Kalogirou 2009). The percentage of installed solar thermal collectors per inhabitant in some cases exceeds one m^2/capita, such as in the case of Cyprus (Kalogirou 2005). The use of solar thermal collectors has proven to be economically viable, which is why today this technology is flourishing in other parts of central and northern Europe, such as Austria and Germany (Eicker et al. 2014). The use of these systems extends to other applications, such as industrial heat production, space heating, etc. (Kylili et al. 2018).

Although these systems are highly efficient, it is a fact that their design rationale was not developed significantly in recent decades. There are evident changes in the use of materials, emphasising properties that enhance durability and improve heat transfer (Jiandong, Hanzhong, and Susu 2015), however in terms of the geometry and connectivity of the solar collectors, research has not evolved. The use of finite elements and computational fluid dynamic (CFD) modelling could intensify the improvement of solar thermal collectors' design, emphasising improving their thermal performance and allowing their integration into the building shell. This is a significant challenge for solar thermal collectors. Unlike Building Integrated Photovoltaics (BIPV), solar thermal systems have inherent difficulties in being integrated into the building shell (Lamnatou et al. 2017); hence to date, their integration applications are minimal.

Solar thermal collectors have gained significant attention and have been widely utilised in southern European and Mediterranean countries, leveraging the abundant solar resources and aiming to meet the increasing demand for renewable energy sources.

Several studies have demonstrated the successful implementation of solar thermal collector systems in the region, primarily for domestic hot water production, space heating, and industrial process heat (Papamanolis 2016). The Mediterranean climate, characterised by long periods of sunshine and high solar radiation, provides favourable conditions for the efficient operation of solar thermal collectors, resulting in substantial energy savings and reduced carbon emissions (Arabzadeh, Jokisalo, and Kosonen 2019). Researchers have explored various types of solar thermal collectors, including flat-plate collectors, evacuated tube collectors, and concentrating collectors, to optimise performance and maximise energy yield in these geographic areas (Papadopoulos et al. 2017). Policy frameworks and incentives, such as feed-in tariffs, tax incentives, and renewable energy targets, have played a crucial role in promoting the widespread adoption of solar thermal collectors in southern European and Mediterranean countries, further accelerating the transition towards clean and sustainable energy systems (Kashani, Izadkhast, and Asnaghi 2014; Mazloum and Ghanem 2022)

This study attempts to shed light on the object of the optimised design of solar thermal systems installed in the building shell, using finite elements and Computational Fluid Dynamic (CFD) modelling. In this work, three different solar thermal systems were numerically tested concerning their energy performance. The study was carried out on the rationale of integrating the collectors into the building in a vertical layout. The work's assumptions allowed the simulation of the building's real conditions, considering the simultaneous consumption of hot water and the possibility of integration into different orientations of the shell for different seasons of the year. The work resumes

calculating temperature and energy profiles produced by various systems, resulting in the optimal conditions and data for the design of building-integrated solar thermal systems.

2. Overview of studies in the numerical analysis of solar thermal collectors

The scientific studies conducted in the numerical assessment of solar thermal plate collectors address different solar collectors under diverse boundary conditions. In recent years, the leading practice in this field is the application of computational fluid dynamics (CFD) models to define the thermal performance of the investigated models. A variety of multi-dimensional models have been developed using various tools and CFD models such as Ansys-Fluent, OpenFoam, COMSOL, Solidworks, Star-CCM, Matlab etc.

- The **CFD models' physics is** mainly based on transport continuity equations, namely the mass, momentum and energy conservation equations. (Ababsa and Bougoul 2017; Andrade Cando, Quitiaquez Sarzosa, and Toapanta 2020; Fertahi et al. 2018; Fowzi 2017; Garnier, Muneer, and Currie 2018; Gunjo, Mahanta, and Robi 2017; Jiandong, Hanzhong, and Susu 2015; Long et al. 2020; Mintsa Do Ango, Medale, and Abid 2013; Nayak et al. 2018; Quitiaquez et al. 2020; Vetter, Fischer, and Dr$\sqrt{}$(ck 2018; Wang et al. 2015). In some studies, the convective and radiative heat transfer and the working fluid's useful gain heat are also employed. (Leone and Beccali 2016; Rangababu, Kiran Kumar, and Srinivasa Rao 2015).
- The **geometry** of the models is that of a flat plate solar thermal collector with an absorber plate. Some studies assume the use of an absorber made of copper. (Fertahi et al. 2018; Gunjo, Mahanta, and Robi 2017; Long et al. 2020). Concerning the size of the geometry, various solar collector sizes are observed regarding length and width. These range from 0.98–2.5 [m] and 0.13–0.98 [m], respectively. The absorber plate thickness ranges from 0.1–2.1 [mm] with two types of absorber configurations, with a squared and rounded circumference. (Jiandong, Hanzhong, and Susu 2015).

Concerning the boundary conditions of the CFD simulations, a range of values and approaches is observed.

- Concerning **weather conditions**, CFD simulations are performed utilising environmental data such as ambient temperature and solar radiation. In some studies, weather data from specific locations are retrieved and employed (Wurzburg, Guangzhou, Fez, Edinburgh, Merida, Sultanate of Oman, Limassol, etc.). Concerning the solar radiation values used as boundary conditions in CFD studies, these range between 120 and 1200 [W/m^2]. In most occasions, steady-state conditions are considered for solar thermal radiation, while transient solar heat flux, varying on an hourly time step, is considered. Although steady-state simulations are much easier to conduct compared to transient studies, the result of the latter presents a better agreement with measured values. The ambient temperature varies from constant to dynamic, ranging from 15 to 37 [°C]. The wind speed is also considered in studies with continuous values ranging from 2 to 14 [m/s].
- The mass flow rate of the thermal medium considered to be in studies is constant and variable. The mass flow rate values range from 0.0125–0.26 [kg/s]. The fluid inlet temperature is not constant, whereas the fluid temperature has constant values ranging from 20 to 45 [°C]. The initial temperature of the thermal medium is also considered.

The investigated studies result in the extraction of the following information:

- the effect of the system geometry (e.g. absorber thickness, the air gap between glass and absorber), the mass flow rate and the materials (e.g. of absorber or pipes) on the system efficiency (Mintsa Do Ango, Medale, and Abid 2013; Wang et al. 2015).

- the useful energy gain and the entropy generation (Fowzi 2017; Rangababu, Kiran Kumar, and Srinivasa Rao 2015).
- the velocity, pressure drop and Reynolds number (Ababsa and Bougoul 2017; Andrade Cando, Quitiaquez Sarzosa, and Toapanta 2020).

Tables 1 and 2 summarise the boundary conditions, the physics and the geometry of the conducted numerical studies in the field of solar thermal collectors assessment.

3. Materials and methods

3.1. Boundary conditions

In this study, a numerical model for the simulation of building-integrated solar thermal collectors' thermal performance was developed. The model was based on the finite element method, and the flow simulation engine of SolidWorks was employed (Dassault Systèmes SOLIDWORKS Corp., n.d.). The analysis was performed for four calendar months (January, March, August and November) for Nicosia, Cyprus, delivering results for all seasons of the year in the four orientations (North, South, West and East) (EU SCIENCE HUB, n.d.). The fluid circulation rate was set based on ISO 12975, and all systems were simulated with forced convection considering a 50-watt typical pump with 8 h of operation per day, with approximately electricity consumption of 1,6 kWh. In this numerical model, the water consumption profile was considered (Department for Environment Food & Rural Affairs 2008) as shown in Figure 1. The specific fluid rate at a given time was subtracted from the system, thus accounting for heat removed from the system, therefore water consumption. In Table 3, the boundary conditions of the simulated models are provided.

Table 1. Boundary conditions that are considered for the numerical simulation.

Study	Boundary Conditions					
	Solar Radiation [W/m^2]	Mass Flow Rate [Kg/s]	Wind Velocity [m/s]	Initial Fluid Temperature [°C]	Inlet Fluid Temperature [°C]	Ambient Temperature [°C]
Jiandong, Hanzhong, and Susu (2015)	700	0.005	4	–	20	15
Vetter, Fischer, and Dr√(ck (2018)	788	0.042	2	–	19.9–79	22
Gunjo, Mahanta, and Robi (2017)	700	0.0125 & 0.025	–	–	15–45	25
Fertahi et al. (2018)	–	0.26	–	60	95	–
Long et al. (2020)	1000	0.01–0.08	–	20	20	22
Garnier, Muneer, and Currie (2018)	400	0.02	–	–	–	20.5
Wang et al. (2015)	800	0.025 & 0.25	–	–	–	–
Leone and Beccali (2016)	Dynamic	Dynamic	–	–	Dynamic	Dynamic
Rangababu, Kiran Kumar, and Srinivasa Rao (2015)	1030	–	1.4 & 2.25	–	–	21.85–25.85
Ababsa and Bougoul (2017)	–	–	–	–	Dynamic	–
Sami, Marin, and Rivera (2016)	Dynamic	–	–	–	–	–
Quitiaquez et al. (2020)	650 & 800	0.02 & 0.1	–	–	–	–
Andrade Cando, Quitiaquez Sarzosa, and Toapanta (2020)	1200	0.0125	2	–	31.85	36.85
Mintsa Do Ango, Medale, and Abid (2013)	350–1200	0.0025 & 0.005	–	–	20,30,40	–
Medina Carril et al. (2016)	786	–	14	–	–	32
Fowzi (2017)	Dynamic	0.0221	–	–	–	–
Nayak et al. (2018)	950	0.004123	–	–	29.85	35
Agathokleous et al. (2019)	121–440	0.02	–	–	–	24

Table 2. Numerical Simulation model characteristics.

Study	Numerical model characteristics					
	Software	Design	Conservation Equations	Location	Collector Type	Collector Dimensions
Jiandong, Hanzhong, and Susu (2015)	–	3D	Mass, Momentum and Energy	Guangzhou, China	Flat Plate	Solar Collector plate thickness: 0.1–2.1 mm
Vetter, Fischer, and Dr√(ck (2018)	Virtcoll + Project	3D	Mass, Momentum and Energy	Wurzburg, Germany	Flat Plate	–
Gunjo, Mahanta, and Robi (2017)	Ansys Fluent	3D	Momentum and Energy	–	Flat Plate / Cooper	Solar Collector length, width: 1.65, 0.1 m Tube diameter, thickness: 0.0125 m,0.007m
Fertahi et al. (2018)	OpenFOAM	3D	Mass, Momentum and Energy	Fez, Mexico	Flat Plate / Cooper	Collector length, external, internal diameter: 1.8 m,58 mm,47mm
Long et al. (2020)	Ansys Fluent	3D	Mass, Momentum and Energy	–	Flat Plate / Cooper	Solar Collector Size: 130 mm x 2 mm x 2000mm
Garnier, Muneer, and Currie (2018)	Ansys Fluent	3D	Momentum and Energy	Edinburgh, UK	Flat Plate	Solar Collector Size: 1400 mm x 700mm
Wang et al. (2015)	Ansys Fluent	3D	Momentum and Energy	Guangzhou, China	Flat Plate	Solar Collector Size: 1960mm x 1000mm
Leone and Beccali (2016)	Comsol	2D & 3D	Convective heat exchange and radiative flux	–	Flat Plate	Solar Collector Length: 2500mm
Rangababu, Kiran Kumar, and Srinivasa Rao (2015)	Ansys Fluent	3D	Useful gain heat	Warangal, India	Flat Plate	Solar Collector Size: 915 mm x 810 mm x 95mm
Ababsa and Bougoul (2017)	Ansys Fluent	3D	Mass, Momentum and Energy	–	Flat Plate	Solar Collector Size: 1360 mm x 680mm
Sami, Marin, and Rivera (2016)	Comsol	3D	Energy and Heat transfer	–	Flat Plate	Solar Collector Size: 1360 mm x 680mm
Quitiaquez et al. (2020)	Ansys Fluent	3D	Mass, Momentum and Energy	–	Flat Plate	Solar Collector length, thickness 960 mm/0.001m
Andrade Cando, Quitiaquez Sarzosa, and Toapanta (2020)	Ansys Fluent	3D	Mass, Momentum and Energy	–	Flat Plate	Solar Collector Size, thickness: 1600 mm x 10 mm /0.001m
Mintsa Do Ango, Medale, and Abid (2013)	Star-CCM	3D	Mass, Momentum and Energy	–	Flat Plate	Module size, thickness: 2000mm x 200 mm/62mm
Medina Carril et al. (2016)	Ansys Fluent	2D	Net heat flow	Merida, Mexico	Flat Plate	–
Fowzi (2017)	Matlab	1D	Mass, Momentum and Energy	–	Flat Plate	Riser Length: 1200mm
Nayak et al. (2018)	Ansys Fluent	3D	Mass, Momentum and Energy	Sultanate of Oman	Flat Plate	Solar Collector size, thickness: 980 mm x 980 mm/10mm
Agathokleous et al. (2019)	Matlab	1D	–	Limassol, Cyprus	Flat Plate	Solar Collector size, thickness: 1631 mm x 846 mm/0.6mm

3.2. Geometry and mesh

Two geometries of solar thermal collectors were investigated, a uniform riser in the size of commercial solar thermal collectors and a group of interconnected risers with an area of 0.4×0.4 m^2 each. Additionally, for the latter geometry, the risers' connectivity was modified, delivering a third alternative geometry. As shown in Table 4, the investigated geometry's main elements were the absorber, the risers, the casing, the thermal insulation, the protective glass, the air between the glass and the absorber, and the tank reservoir. An overview of the investigated geometries and information and drawings of the investigated domain mesh are provided in Table 4.

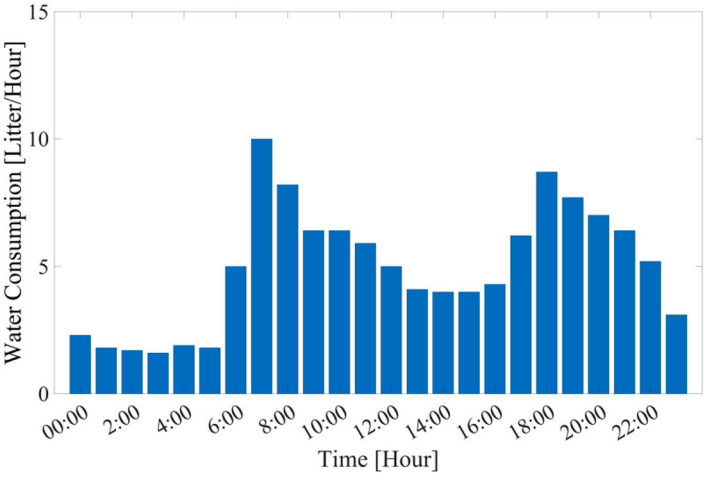

Figure 1. Water Consumption [L/h] Versus Time [h].

Table 3. Boundary Conditions.

Property	Value	Units
Thermal medium mass flow rate	0.038	[kg/s]
Solar thermal radiation	Transient (Georgiou et al. 2021)	[W/m^2]
Ambient Temperature	Transient (Georgiou et al. 2021)	[°C]
Water consumption profile	Transient (Figure 1)	[kg/s]
Water initial temperature	Regulated (24 h initial operation)	[°C]
Inclination	0,45,90	°

The curvature level regarding the domain mesh was set to be at 0.5548, and the tolerance criterion value was 0.0005 m. The mesh preset was set at level two, which corresponds to the cell density in regions. Based on a preliminary study with different presets, this refinement level was decided, according to which this mesh domain delivered reliable results in a shorter time Table 5.

The solar collector models were incorporated vertically into a building masonry structure. A thermal assessment was performed, and the heat transferred through the masonry structure was investigated. Information regarding the building-integrated solar collector system materials is provided in Table 6, and an overview of the model is shown in Figure 2. Also, the velocity profile of each system is illustrated in Figures 3–5.

3.3. Governing equations

The physics employed for the numerical analysis was based on transient heat transfer principles and fluid dynamics. The absorber was particularly subjected to non-steady solar radiation, and heat transfer due to conduction was assumed between the absorber and the riser. Thermal losses due to the convection of the fluid in the riser were also considered. The governing equations employed were the mass, momentum and energy conservation laws, based on the Navier-Strokes approach, for closed-loop forced circulation, expressed as follows:

$$\frac{\partial \rho}{\partial t} + \frac{\partial (\rho u_i)}{\partial x_i} = 0 \tag{1}$$

$$\frac{\partial (\rho u_i)}{\partial t} + \frac{\partial}{\partial x_j}(\rho u_i u_j) + \frac{\partial P}{\partial x_i} = \frac{\partial}{\partial x_j}(\tau_{ij} + \tau_{ij}^R) + S_i \tag{2}$$

$$\frac{\partial \rho H}{\partial t} + \frac{\partial \rho u_i H}{\partial x_i} = \frac{\partial}{\partial x_i}(u_j(\tau_{ij} + \tau_{ij}^R) + q_i) + \frac{\partial \rho}{\partial t} - \tau_{ij}^R \frac{\partial u_i}{\partial x_j} + \rho\varepsilon + S_i u_i + Q_H \tag{3}$$

$$H = h + \frac{u^2}{2} \tag{4}$$

Concerning the solid regions of the model, heat conduction was assumed:

$$\frac{\partial \rho e}{\partial t} = \frac{\partial}{\partial x_i}\left(\lambda_i \frac{\partial T}{\partial x_i}\right) + Q_H \tag{5}$$

3.4. Numerical model validation

The numerical model employed in this study was validated with the use of experimental data published by (Souliotis 2021). The geometry and boundary conditions described in (Souliotis 2021) were developed, as well as the physics of the numerical model implemented in this study was applied. The boundary conditions of the validation model were the specified riser input fluid temperature, the ambient temperature and the solar radiation. For the validation of the numerical (N) and experimental values (E), the root mean square deviation formula was incorporated.

Table 4. Investigated Configurations – Domains.

System	Model configuration	Domain Mesh	Mesh Information
Uniform Riser	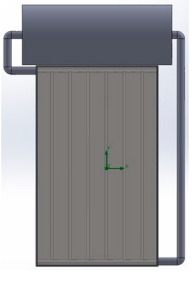	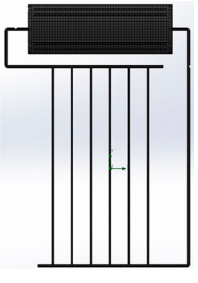	Size of cells per X: 0.0841 (m) Size of cells per Y: 0.0845 (m) Size of cells per Z: 0.0841 (m) Minimum gap size: 0.0222 (m) Total Cells: 423,235 Fluid Cells: 230,906 Solid Cells: 192,329 Fluid Cells contacting solids: 101,890
Multiple Riser Configuration One	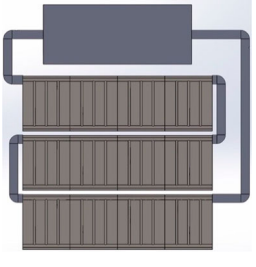	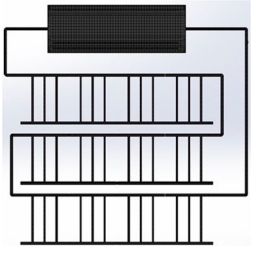	Size of cells per X: 0.0866 (m) Size of cells per Y: 0.0941 (m) Size of cells per Z: 0.0841 (m) Minimum gap size: 0.0222 (m) Total Cells: 707,507 Fluid Cells: 353,310 Solid Cells: 354,197 Fluid Cells contacting solids: 181,007
Multiple Riser Configuration Two	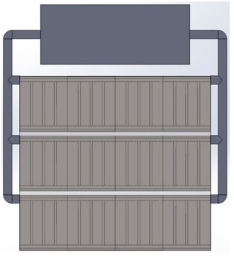	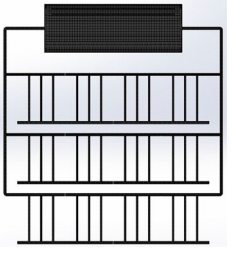	Size of cells per X: 0.0853 (m) Size of cells per Y: 0.0862 (m) Size of cells per Z: 0.0841 (m) Minimum gap size: 0.0222 (m) Total Cells: 655,434 Fluid Cells: 327,807 Solid Cells: 327,627 Fluid Cells contacting solids: 167,792

Table 5. Investigated Configurations – Domains (cont'd).

Riser	Riser Configuration	Fluid Flow Illustration	System Description
Uniform Riser	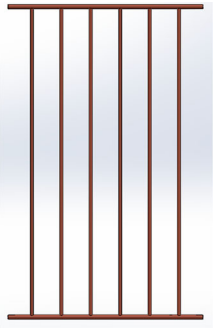	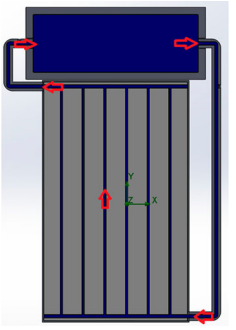	Uniform riser One inlet One outlet
Multiple Riser Configuration One	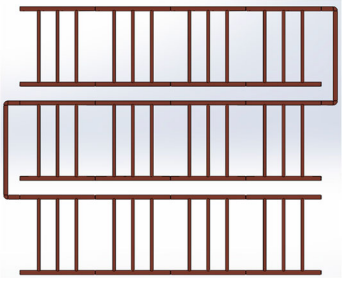	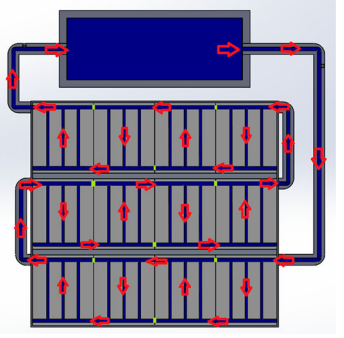	Three groups of risers assembly. Each group consists of four individual risers. Each riser has one inlet and one outlet. Fluid flows through the first group, then to the second, then to the third and then back to the tank inlet.
Multiple Riser Configuration Two	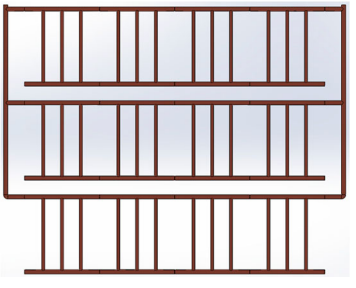	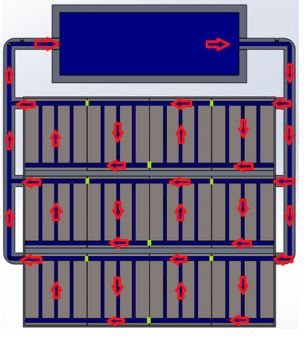	Three groups of risers assembly. Each group consists of four individual risers. Three inlets, three outlets Fluid flows simultaneously through all three riser groups and exits towards the tank inlet.

$$\mathrm{RMSD} = \sqrt{\frac{\sum_{i=1}^{n} (N_i - E_i)^2}{n}} \tag{6}$$

4. Results

In this section, a brief overview of all investigated systems is presented. The roof-installed systems are exposed to significantly higher solar radiation due to their position. The fluid temperature difference gap between uniform and multiple riser configurations is narrowed Table 7 presented slope 0° simulation results. The maximum average fluid temperature difference is marked under autumn conditions between the uniform riser and multi-riser configuration. Identical thermal behaviour between multi-riser setups is obtained, further designating that the fluid temperature

Table 6. Building-Integrated Solar Collector Materials.

Solar Collector						
Component Description	Material	Thermal Conductivity [W/(m·K)]	Heat Capacity [J(Kg·K)]	Density [kg/m^3]	Thickness [cm]	Dimensions [m]
Front case cover	Glass	0.74976	834.61	2457.6	0.20	1.66 [L] x 1[W]
Case	Aluminium	200	900	2700	10.00	1.68 [L] x 1.02 [W]
Riser	Cooper	390	390	8900	0.09	1.6 [L] x 1 [W]
Pipes	Cooper	390	390	8900	0.09	Variable
Pipes Insulation	Polyurethane	0.05	1500	70	2.00	Variable
Tank	Cooper	390	390	8900	0.09	1.16 [L] x 1.34 [Perimeter]
Tank Insulation	Mineral Wool	0.035	837	70	5.00	1.25 [L] x 1.8 [Perimeter]
Case insulation	Mineral Wool	0.035	837	70	5.00	1.57 [L] x 1 [W]
Masonry Wall						
Component Description	**Material**	**Thermal Conductivity [W/(m·K)]**	**Heat Capacity [J(Kg·K)]**	**Density [kg/m^3]**	**Thickness [cm]**	**Dimensions [m]**
Exterior	Mortar Plaster	1.000	1000	700	2.50	1.68 [L] x 1.02 [W]
Interior	Mortar Plaster	1.000	1000	700	2.50	1.68 [L] x 1.02 [W]
Brick	Hollow Brick	0.400	900	880	20.00	1.68 [L] x 1.02 [W]
Brick Air Holes	Air	0.025	1008	1.23	20.00	5 × 5

gap is much lower than the slope of 90°. Even though slope 0° displayed inferior thermal performance compared to slope 45°, it achieved the maximum fluid temperature of 54 [°C], which was considered the highest of all. According to the slope 45° simulation results in Table 8, the optimal

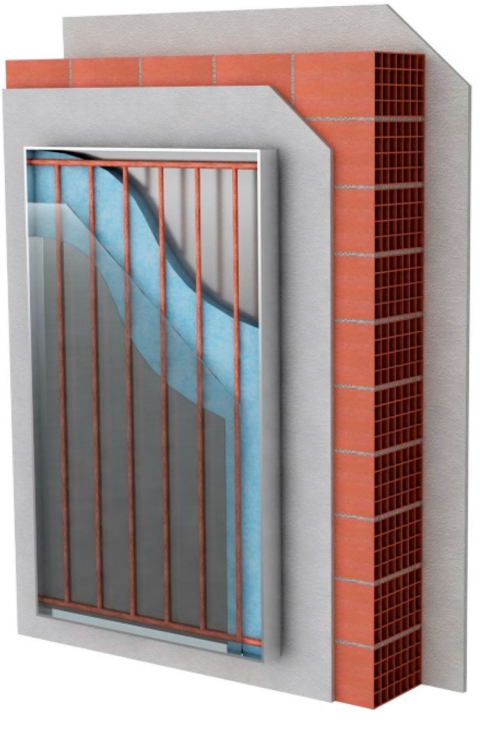

Figure 2. Building-integrated Solar Collector Structure.

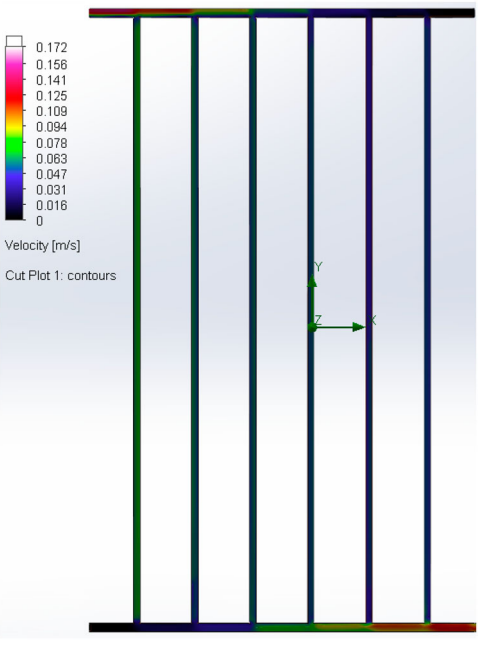

Figure 3. Riser Fluid Velocity – Uniform Riser.

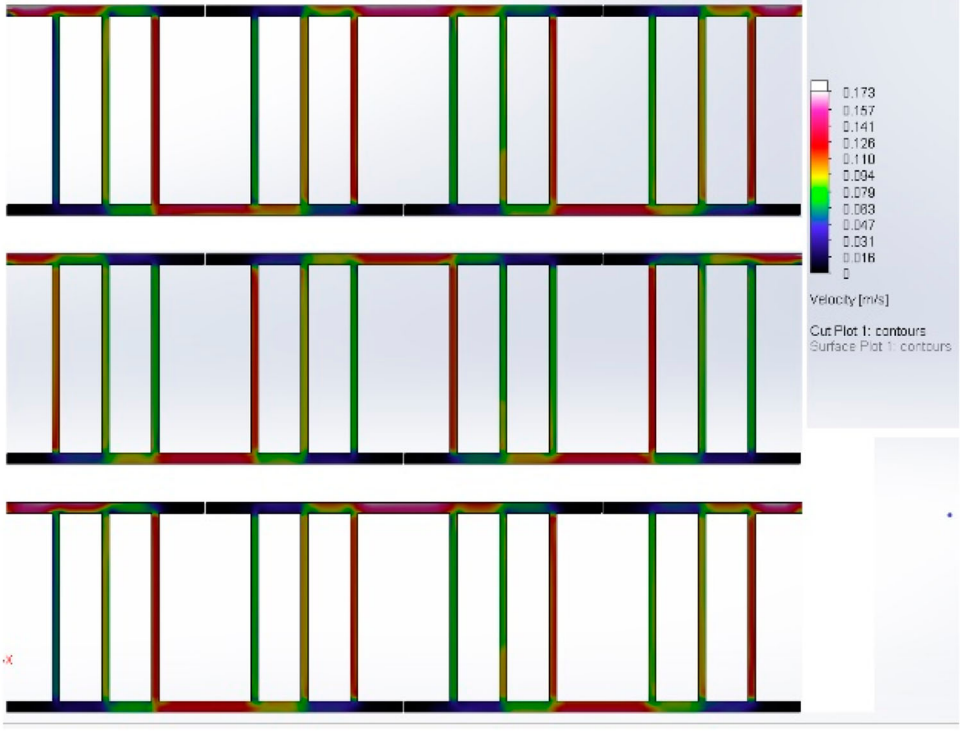

Figure 4. Riser Fluid Velocity – Multiple Riser Configuration One.

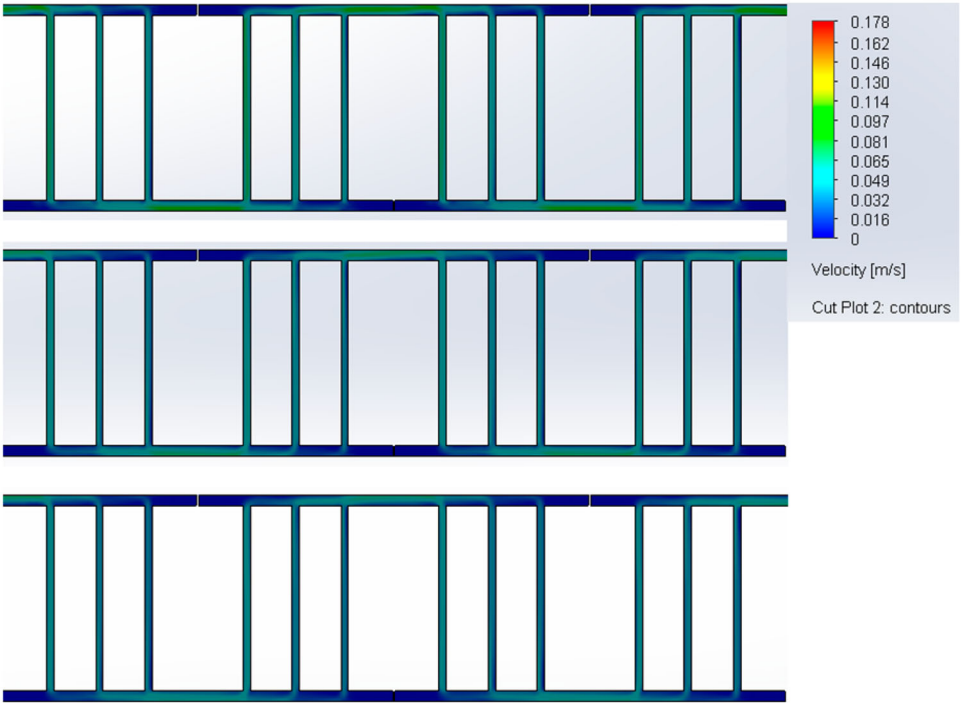

Figure 5. Riser Fluid Velocity – Multiple Riser Configuration Two.

orientation for maximum thermal performance is south. Concerning all seasons Table 9 presents the results obtained for slope 90°, and the south orientation provided the best performance under autumn, winter, and spring conditions and the east orientation for the summer season. Regarding the BIST results presented in Figure 12, the maximum heat flux occurred in winter conditions and the lowest in spring with a value of 141.55 [W/m^2] and −56.03 [W/m^2] respectively. The full set of data for this numerical study considering all the hourly average fluid temperature, hourly heat flux, hourly solar radiation and ambient temperature for all investigated dynamic conditions is provided. (Georgiou et al. 2021).

4.1. Numerical model validation

The numerical and experimental temperature profile comparison is presented in Figure 6 which indicated a good agreement between the two. The calculated value from the root mean square deviation formula (RMSD) for the experimental and numerical cases is 5.01% which is considered acceptable (Pawar and Sobhansarbandi 2020).

Table 7. Minimum, average and maximum – System fluid temperatures [°C] at Slope 0°.

	Uniform Riser			Multiple Riser Configuration One			Multiple Riser Configuration Two		
	Min [°C]	Average [°C]	Max [°C]	Min [°C]	Average [°C]	Max [°C]	Min [°C]	Average [°C]	Max [°C]
Autumn	21.09	22.37	23.84	24.87	28.88	33.74	23.36	26.22	29.69
Winter	14.72	16.38	18.26	15.60	17.87	20.43	15.60	17.84	20.39
Spring	21.86	25.93	30.72	24.17	29.93	36.78	24.19	29.91	36.73
Summer	35.07	40.15	45.91	37.96	45.47	54.00	38.00	45.46	53.90

Table 8. Minimum, average and maximum – System fluid temperatures [°C] at Slope 45°.

		Uniform Riser			Multiple Riser Configuration One			Multiple Riser Configuration Two		
		Min [°C]	Average [°C]	Max [°C]	Min [°C]	Average [°C]	Max [°C]	Min [°C]	Average [°C]	Max [°C]
Autumn	South	25.59	30.05	35.25	27.97	34.36	42.07	27.99	34.36	41.98
	West	23.08	25.60	28.96	24.52	28.03	32.67	24.51	28.01	32.63
	North	20.67	21.65	22.80	21.09	22.37	23.84	21.08	22.36	23.83
	East	22.79	25.65	28.56	24.04	28.05	32.20	24.05	28.04	32.16
Winter	South	15.80	18.15	20.84	17.10	20.38	24.13	17.09	20.33	24.04
	West	14.59	16.04	17.84	15.42	17.39	19.82	15.41	17.36	19.77
	North	13.53	14.39	15.33	13.94	15.06	16.28	13.93	15.04	16.27
	East	14.50	16.11	17.77	15.25	17.47	19.75	15.26	17.44	19.70
Spring	South	23.00	27.78	33.46	25.71	32.63	40.91	25.75	32.61	40.85
	West	21.30	24.80	29.45	23.42	28.36	34.91	23.40	28.34	34.97
	North	18.17	19.90	21.88	19.08	21.38	24.01	19.09	21.37	23.97
	East	20.89	24.85	28.84	22.80	28.38	34.09	22.81	28.38	34.03
Summer	South	34.46	39.49	45.21	37.19	44.53	52.96	37.25	44.51	52.92
	West	34.33	38.52	44.26	37.03	43.18	51.55	37.03	43.15	51.54
	North	32.48	35.65	39.10	34.48	38.97	43.88	34.49	38.94	43.82
	East	33.62	38.79	43.73	36.02	43.51	50.88	36.01	43.49	50.80

Table 9. Minimum, average and maximum – System fluid temperatures [°C] at Slope 90°.

		Uniform Riser			Multiple Riser Configuration One			Multiple Riser Configuration Two		
		Min [°C]	Average [°C]	Max [°C]	Min [°C]	Average [°C]	Max [°C]	Min [°C]	Average [°C]	Max [°C]
Autumn	South	25.00	28.98	33.61	27.12	32.89	39.74	27.16	32.81	39.50
	West	22.03	23.78	26.22	23.02	25.44	28.80	23.00	25.40	28.71
	North	20.20	20.90	21.71	20.44	21.32	22.32	20.43	21.30	22.29
	East	21.71	23.82	25.78	22.55	25.48	28.23	22.57	25.43	28.14
Winter	South	15.45	17.54	19.91	16.59	19.52	22.84	16.60	19.46	22.71
	West	13.98	15.01	16.33	14.56	15.94	17.68	14.55	15.91	17.63
	North	13.12	13.66	14.24	13.33	14.04	14.79	13.32	14.03	14.77
	East	13.83	15.00	16.12	14.34	15.94	17.46	14.35	15.90	17.40
Spring	South	20.92	24.42	28.52	22.89	27.83	33.67	21.95	26.59	32.21
	West	19.55	21.85	25.16	20.98	24.19	28.77	19.78	22.91	27.37
	North	16.81	17.75	18.80	17.17	18.34	19.66	16.15	17.09	18.28
	East	18.94	21.76	24.21	20.15	24.10	27.57	19.13	22.82	26.13
Summer	South	30.81	34.06	37.67	32.39	36.27	40.70	32.40	36.21	40.58
	West	31.97	35.19	40.18	33.81	37.83	43.86	33.79	37.76	43.63
	North	28.91	30.12	31.37	29.52	30.88	32.30	29.53	30.85	32.25
	East	31.04	35.22	38.98	32.74	37.90	42.58	32.74	37.83	42.42

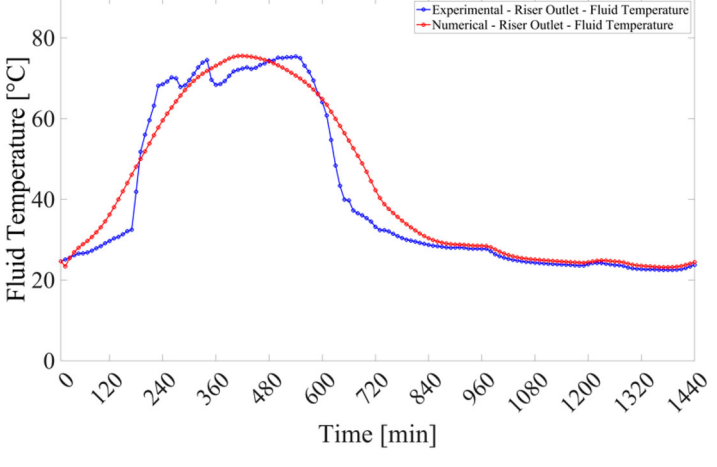

Figure 6. Experimental Vs Numerical – Riser Outlet – Fluid Temperature.

4.2. Assessment of system performance by considering water consumption

The simulated results of the fluid temperature profiles are presented in Figures 7 and 8 under two scenarios, including and excluding water consumption. The first case involving water consumption resulted in lower fluid temperatures since the hot water was being removed from the tank reservoir; thus, the temperature decreased. A higher fluid temperature is achieved when water consumption is not considered. The consumption of hot water represents realistic conditions; to this end, this parameter's inclusion resulted in more reliable results.

In winter conditions, the temperature difference between the two scenarios was higher due to the lower environmental temperatures and the reduced heat transfer due to solar radiation. In contrast, the temperature difference in summer conditions is lower since the solar collector is exposed to prolonged solar radiation times, and the ambient temperature is considerably higher.

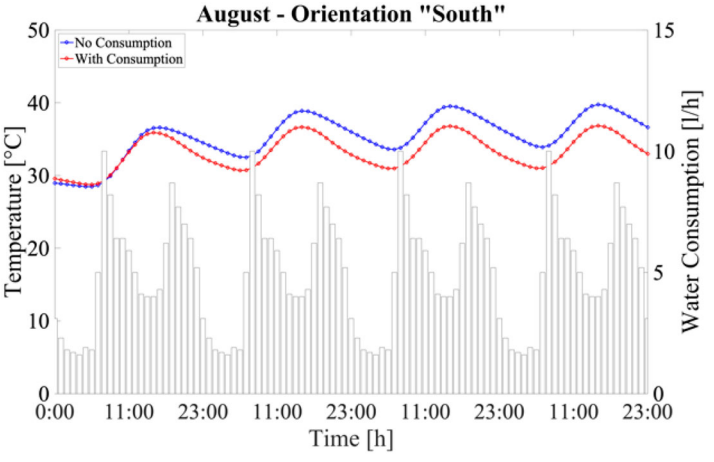

Figure 7. System Average Fluid Temperature – Multiple Riser Configuration One – Water Consumption Comparison – August – South – Slope 90° – Last 24 h.

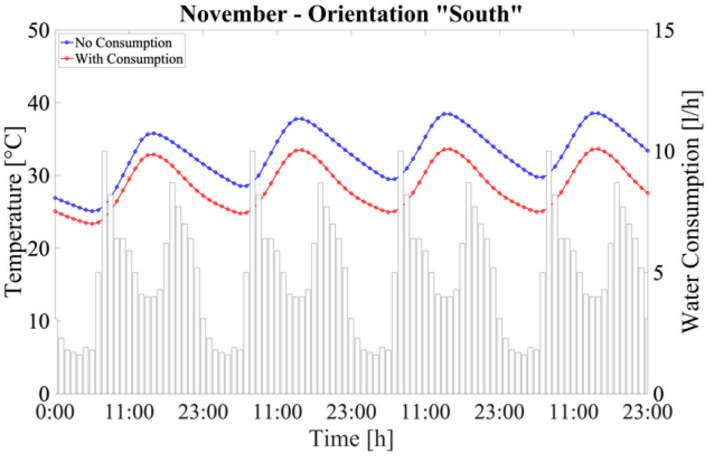

Figure 8. System Average Fluid Temperature – Multiple Riser Configuration One – Water Consumption Comparison – November – South – Slope 90° – Last 24 h.

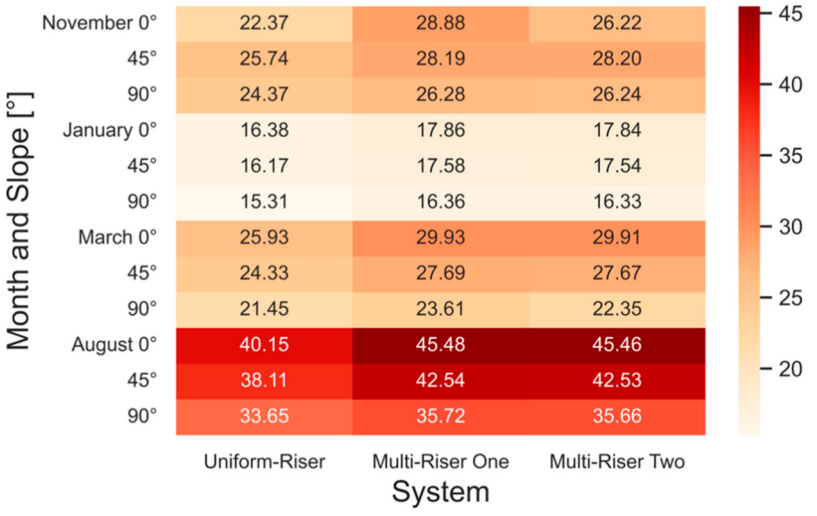

Figure 9. Average System Temperature [°C] – All Months, Slope 0°,45° and 90°.

4.3. Assessment of uniform and multiple risers

The thermal analysis of the fluid temperature regarded the three solar collector model configurations are shown in Figure 9. The uniform riser system delivered the lowest fluid temperature; in contradiction, the multiple riser model configurations proved to be more efficient with multi-riser configuration one to have achieved the highest fluid temperature even higher when compared to multi-riser configuration two. The improvement of thermal performance in a multiple riser model was attainable because of the larger area of the riser, which resulted in higher efficiency of solar radiation absorption. It should be stated that the overall dimensions of both systems' absorbers are the same. Thus, although it does not require more space, the multiple risers' solution results in a more effective system. The fluid flow pattern is a critical factor for collector systems, affecting thermal performance and should be considered.

4.4. The impact of the orientation on thermal performance

The thermal performance simulation results presented in Figures 10 and 11 considered the orientation under diverse weather conditions. The best thermal performance regarded winter and summer conditions in the south and west orientation, respectively. The lowest fluid temperature is observed to occur in the north orientation in all cases; consequently, it can be extracted that the north orientation for the proposed system should be avoided. The west and east orientation thermal performances were identical. A slight time shift is observed in winter conditions. Still, a considerably bigger occurred in summer, which indicated that a solar collector with a tracking system could increase the overall efficiency. These results come as no surprise and occur due to the solar angle, which delivers better outcomes for these two orientations than the south orientation. However, in the south, the solar exposure time is higher.

4.5. Assessment of roof installed system

In the study, solar thermal collectors' performance on the buildings' roofs for slope angles of 0° and 45° was investigated. The thermal performance simulation results for January and July are presented in Figure 9. In summer conditions, the slope's fluid temperature is 0°, and 45° is considerably higher than 90° due to the significant increase in solar radiation. Contrary to the summer situation's

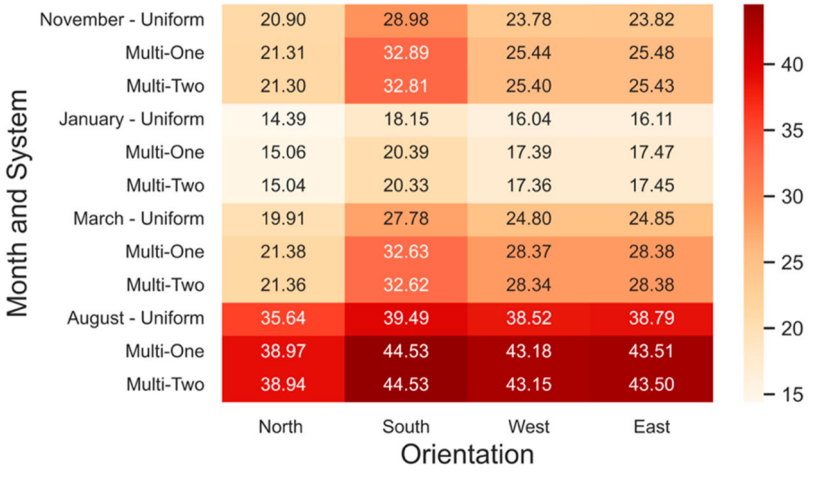

Figure 10. Average System Temperature [°C] Vs Orientation – All Months, Slope 45°.

performance difference, the results under winter conditions showed that vertical collectors have identical thermal performance with roof-installed solar collectors. Despite that, the roof-installed systems with slopes 0° and 45° outperform the integrated solar collectors, but there is great potential since the difference in fluid temperatures is not much apart.

4.6. The impact of the building-integrated solar collector on the building performance

The results considering the implications of BIST on the building wall thermal performance are presented in Figure 12. It is possible to conclude that the BIST acts as a heat source on the building wall justified by the outwards heat flux. When comparing the case of no solar collector integration, the outwards heat flux values are presented, meaning that heat escapes the building. Due to the water's heat capacity and insulation, the BIST system acts as a thermal mass, releasing heat even when there is no solar radiation present. Depending on the environmental conditions, BIST's heat is considered an advantage because it contributes to the overall indoor temperature regulation. It minimises heat released into the environment by acting as a shield barrier and supplying heat. However, as shown

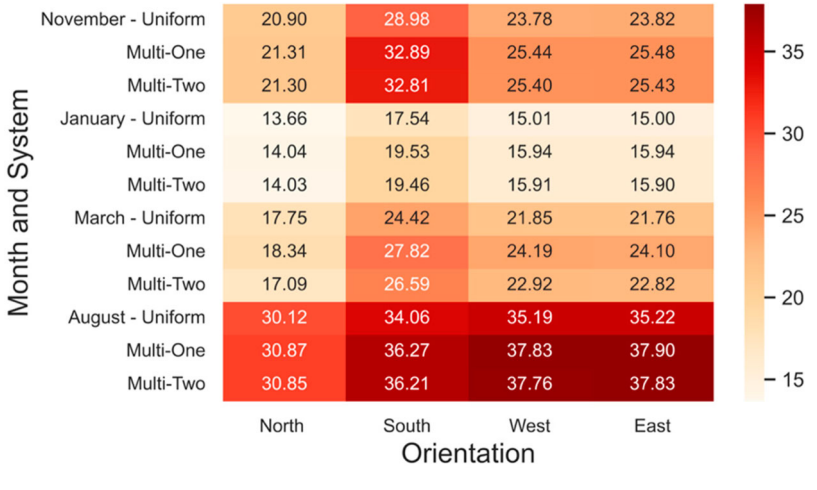

Figure 11. Average System Temperature [°C] Vs Orientation – All Months, Slope 90°.

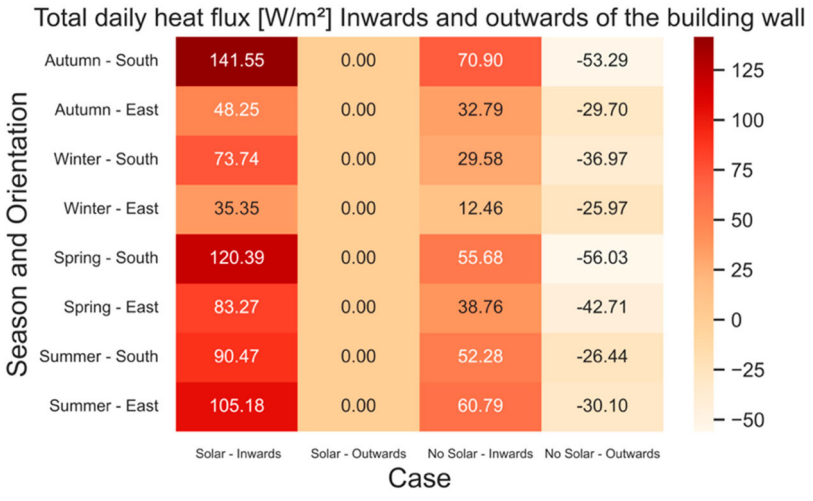

Figure 12. Total daily Heat flux [W/m^2] Inwards and Outwards of the building wall – Building Integrated Solar Collector Vs No Solar Collector.

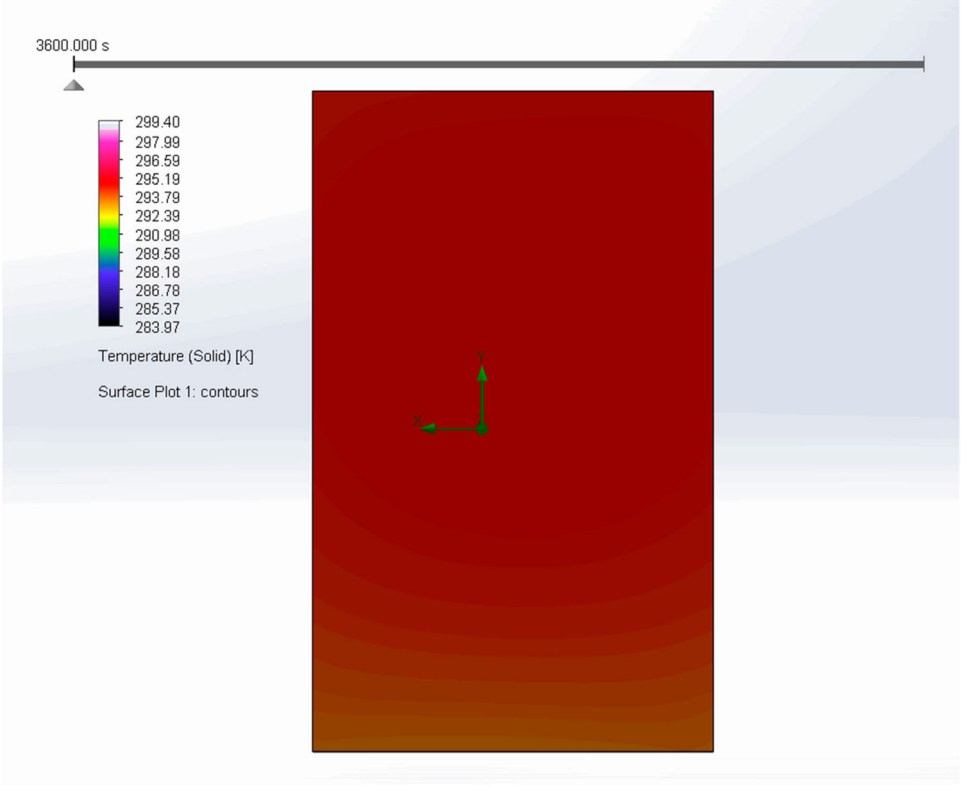

Figure 13. Temperature distribution [K] Outer surface of the collector end in the area in contact with the building envelope – System 2A – August – South Orientation.

in Figure 12, there is also heat flux inwards the building in the summer season. Consequently, BIST system implementation has both advantages and disadvantages for the building. Positively, it adds to the building's existing heat supply, hence improving thermal comfort in general. Improved

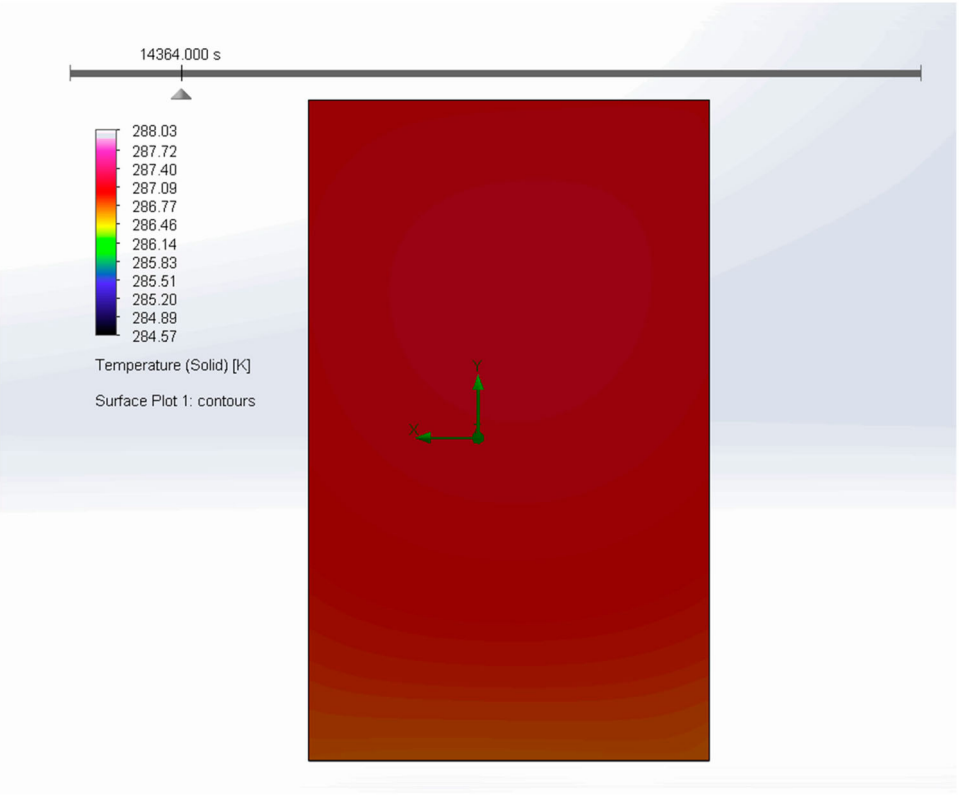

Figure 14. Temperature distribution [K] Outer surface of the collector end in the area in contact with the building envelope – System 2A – March – South Orientation.

energy efficiency is a result of the BIST system's ability to keep heat from escaping the structure. The enhanced heat retention of the BIST system, on the other hand, negatively impacts the building's cooling loads. It hinders the heat's natural dissipation, making it harder to maintain cooler indoor temperatures in the summer. The building's cooling loads are adversely impacted as a result. Given a comparison of the heat flux values between the two situations, it is clear that the BIST system regularly produces heat flux values that are substantially greater.

5. Discussion

This study examined a plate solar collector system's thermal performance integrated into a building shell under diverse weather conditions. Three transient models were developed based on (FEM) in the CFD tool (Dassault Systèmes SOLIDWORKS Corp., n.d.), one model with a uniform riser, and two models with multiple risers assembled. The dynamic operating parameters considered during the simulation were the solar collector's inclination angle, environmental temperature and solar radiation intensity.

Numerical simulation results illustrated each model's fluid temperatures during north, south, west and east orientations. The multiple riser models demonstrated superior thermal performance over the uniform riser configuration, which proved to be a beneficial resolution for improving overall efficiency. The inlet and outlet modifications on the multiple riser model showed a non-significant decrease in fluid temperature, therefore displaying an inferior thermal performance. A critical component of the solar collector system is a riser, which was investigated and revealed to impact the

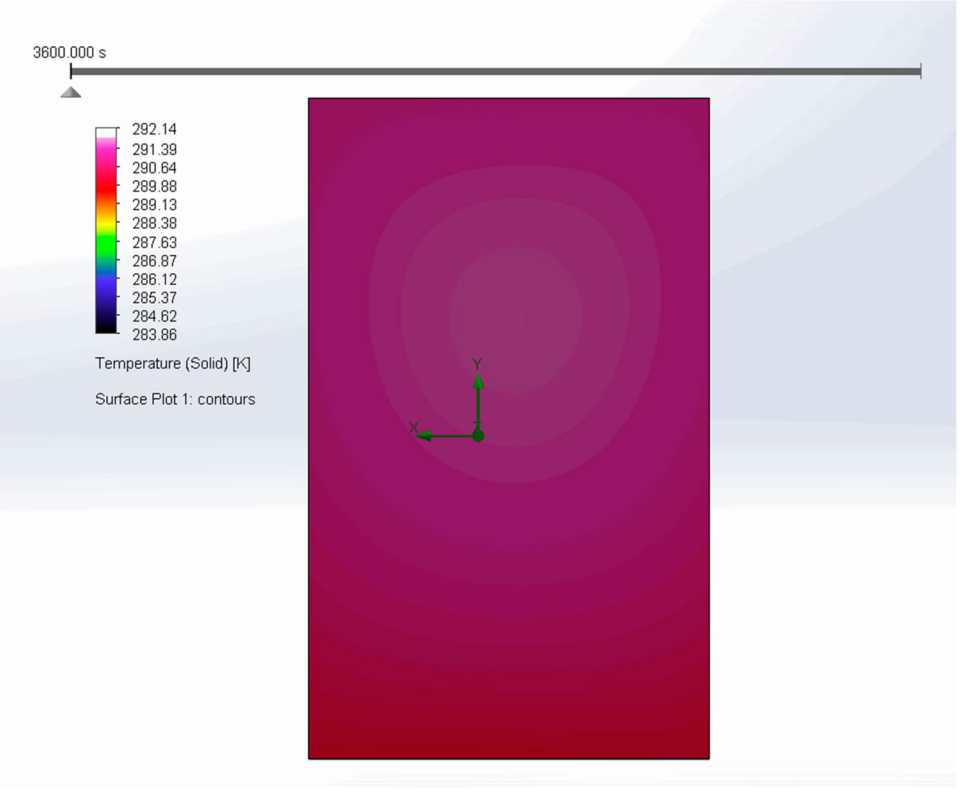

Figure 15. Temperature distribution [K] Outer surface of the collector end in the area in contact with the building envelope – System 2A – November – South Orientation.

efficiency directly. The water consumption factor was considered in all the simulations, and a preliminary numerical simulation presented the impact of water consumption on the accuracy of the results Figures 13–16.

A crucial outcome of building-integrated solar collectors' feasibility and performance is delivered using numerical simulations of various slopes. The building-integrated solar collectors act as a thermal mass and potentially can contribute to the heating and cooling of a building during different seasons.

The novelty of this paper lies in the investigation of building-integrated solar flat collectors with both uniform and multiple riser structures, and their thermal performance under various operating parameters and weather conditions. The study utilises numerical simulations and finite element analysis to evaluate the efficiency and fluid temperatures of different collector configurations. The findings demonstrate the superiority of multiple riser models in terms of thermal performance and highlight the potential of building-integrated solar collectors to contribute to the heating and cooling of buildings throughout different seasons.

Further investigation can be conducted to optimise the design and arrangement of multiple risers in building-integrated solar collectors. This could involve exploring different geometries, sizes, and orientations of the risers to maximise thermal performance and overall efficiency. Also future research can focus on the integration of building-integrated solar collectors with heating, ventilation, and air conditioning (HVAC) systems. This would involve studying the feasibility and effectiveness of utilising the thermal mass of the collectors for heating and cooling purposes, and developing control strategies to optimise energy management within the building.

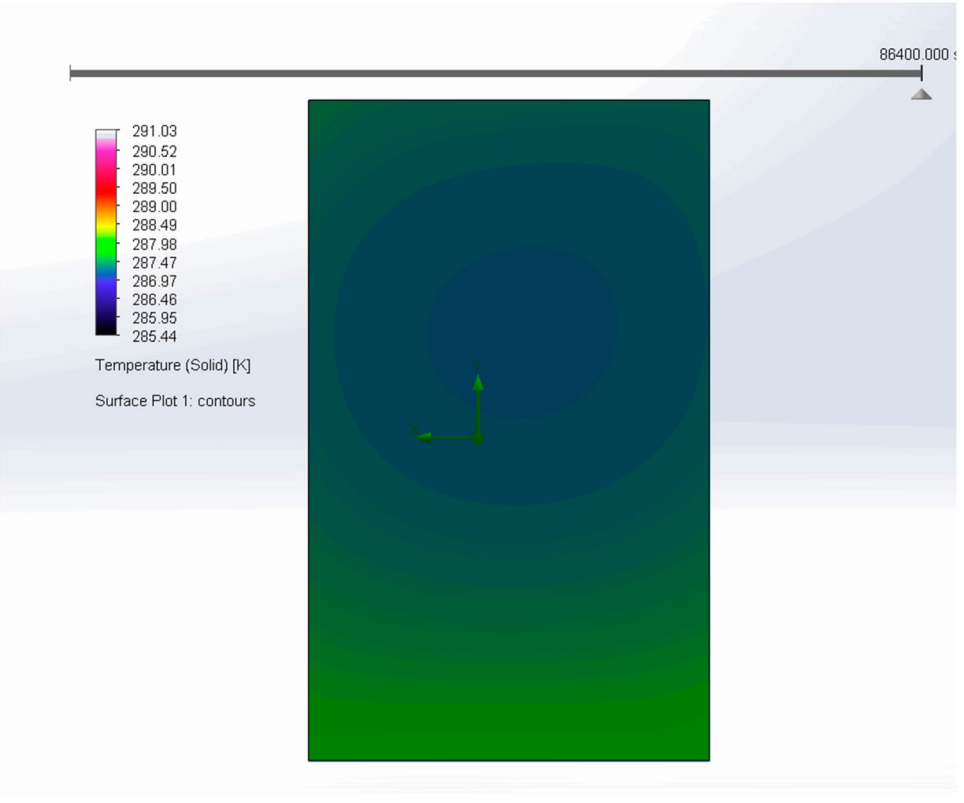

Figure 16. Temperature distribution [K] Outer surface of the collector end in the area in contact with the building envelope – System 2A – January – South Orientation.

Data availability statement

The data that support the findings of this study are openly available in Mendeley Data and Zenodo at http://doi.org/10.17632/xcpyjj2gv7.2 and http://doi.org/10.5281/zenodo.5284639 respectively.

Disclosure statement

No potential conflict of interest was reported by the author(s).

ORCID

Manolis Souliotis http://orcid.org/0000-0001-5779-7805
Paris A. Fokaides http://orcid.org/0000-0003-4112-3819

References

Ababsa, D., and S. Bougoul. 2017. "Numerical Analysis of Thermal and Dynamic Behavior of a Roof Solar Collector." *Heat Transfer-Asian Research* 46. https://doi.org/10.1002/htj.21224.

Agathokleous, R., G. Barone, A. Buonomano, C. Forzano, S. A. Kalogirou, and A. Pal-ombo. 2019. "Building Façade Integrated Solar Thermal Collectors for air Heating: Exper-Imentation, Modelling and Applications." *Applied Energy* 239: 658–679. https://doi.org/10.1016/j.apenergy.2019.01.020.

Andrade Cando, A. X., W. Quitiaquez Sarzosa, and L. F. Toapanta. 2020. "CFD Analysis of a Solar Flat Plate Collector with Different Cross Sections." *Enfoque UTE* 11. doi:10.29019/enfoque.v11n2.601.

Arabzadeh, V., J. Jokisalo, and R. Kosonen. 2019. "A Cost-optimal Solar Thermal System for Apartment Buildings with District Heating in a Cold Climate." *International Journal of Sustainable Energy* 38 (2): 141–162.
Dassault Syst√®mes SOLIDWORKS Corp. n.d. SOLIDWORKS¬Æ CAD software [WWW Document]. Accessed 10 December 2022. https://www.solidworks.com.
Department for Environment Food & Rural Affairs. 2008. Measurement of Domestic Hot Water Consumption in Dwellings.
Eicker, U., D. Pietruschka, M. Haag, and A. Schmitt. 2014. "Energy and Economic Performance of Solar Cooling Systems World Wide." *Energy Procedia* 57. https://doi.org/10.1016/j.egypro.2014.10.269.
EU SCIENCE HUB. n.d. Photovoltaic Geographical Information System (PVGIS) [WWW Document]. URL https://ec.europa.eu/jrc/en/pvgis (accessed 10.12.22).
Fertahi, S. ed-D., T. Bouhal, T. Kousksou, A. Jamil, and A. Benbassou. 2018. "Experimental Study and CFD Thermal Assessment of Horizontal hot Water Storage Tank Integrating Evacuated Tube Collectors with Heat Pipes." *Solar Energy* 170. https://doi.org/10.1016/j.solener.2018.05.062.
Fowzi, M. 2017. CFD Simulation of Enhancement Techniques in Flat Plate Solar Water Collectors.
Garnier, C., T. Muneer, and J. Currie. 2018. "Numerical and Empirical Evaluation of a Novel Building Integrated Collector Storage Solar Water Heater." *Renewable Energy* 126. https://doi.org/10.1016/j.renene.2018.03.041.
Georgiou, L., M. Souliotis, S. Papaefthimiou, and P. A. Fokaides. 2021. "Numerical Simulation Data of Building Integrated Solar Thermal Collectors Under Diverse Conditions." *Data in Brief* 39. https://doi.org/10.1016/j.dib.2021.107470.
Gunjo, D. G., P. Mahanta, and P. S. Robi. 2017. "CFD and Experimental Investigation of Flat Plate Solar Water Heating System Under Steady State Condition." *Renewable Energy* 106. https://doi.org/10.1016/j.renene.2016.12.041.
Jiandong, Z., T. Hanzhong, and C. Susu. 2015. "Numerical Simulation for Structural Parameters of Flat-Plate Solar Collector." *Solar Energy* 117. https://doi.org/10.1016/j.solener.2015.04.027.
Kalogirou, S. A. 2005. Solar Water Heaters in Cyprus: Manufacturing, Performance and Applications.
Kalogirou, S. A. 2009. *Solar Energy Engineering*. Elsevier. https://doi.org/10.1016/B978-0-12-374501-9.X0001-5.
Kashani, A. H., P. S. Izadkhast, and A. Asnaghi. 2014. "Mapping of Solar Energy Potential and Solar System Capacity in Iran." *International Journal of Sustainable Energy* 33 (4): 883–903.
Kylili, A., P. A. Fokaides, A. Ioannides, and S. Kalogirou. 2018. "Environmental Assessment of Solar Thermal Systems for the Industrial Sector." *Journal of Cleaner Production* 176. https://doi.org/10.1016/j.jclepro.2017.12.150.
Lamnatou, C., I. Farkas, Z. Aggelos, A. Buonomano, A. Palombo, and D. Chemisana. 2017. Modelling and performance analysis of building integrated solar thermal (BIST) system. pp. 103-132.
Leone, G., and M. Beccali. 2016. "Use of Finite Element Models for Estimating Thermal Performance of Façade-Integrated Solar Thermal Collectors." *Applied Energy* 171. https://doi.org/10.1016/j.apenergy.2016.03.039.
Long, J., J. Lu, M. Jiang, A. Du, R. Zhang, and A. Yongga. 2020. "Study on Solar Energy Utilization Characteristics of a Solar Building Integrated Wall." *Applied Thermal Engineering* 175. https://doi.org/10.1016/j.applthermaleng.2020.115289.
Mazloum, Y., and A. Ghanem. 2022. "Dynamic modelling of a ground-coupled solar ejector cooling system." *International Journal of Sustainable Energy* 41 (11): 1903–1937.
Medina Carril, D. M., J. G. Carrillo, R. D. Maldonado, and F. Avilés. 2016. "Finite ele-ment Analysis of a Solar Collector Plate Using two Plate Geometries." *Ingeniería e Investi-Gación* 36 (3): 95–101. https://doi.org/10.15446/ing.investig.v36n3.56071
Mintsa Do Ango, A. C., M. Medale, and C. Abid. 2013. "Optimization of the Design of a Polymer Flat Plate Solar Collector." *Solar Energy* 87. doi:10.1016/j.solener.2012.10.006.
Nayak, Nagaraj, A. Anarghya, V. N. Abhishek, and Nasser Al Ghufaili. 2018. "Numerical and Experimental Investigation on Low Cost Solar Water Heater for Ruralareas of Oman." *MOJ Solar and Photoenergy Systems* 2 (2): 43–48.
Papadopoulos, A., T. Tsoutsos, M. Frangou, K. Kalaitzakis, N. Stefanakis, and A. G. Boudouvis. 2017. "Innovative Optics for Concentrating Photovoltaic/Thermal (CPVT) Systems–the Case of the PROTEAS Solar Polygeneration System." *International Journal of Sustainable Energy* 36 (8): 775–786.
Papamanolis, N. 2016. "An Overview of Solar Energy Applications in Buildings in Greece." *International Journal of Sustainable Energy* 35 (8): 814–823.
Pawar, V. R., and S. Sobhansarbandi. 2020. "CFD Modeling of a Thermal Energy Storage Based Heat Pipe Evacuated Tube Solar Collector." *Journal of Energy Storage* 30. https://doi.org/10.1016/j.est.2020.101528.
Quitiaquez, W., J. Estupi√±an-Campos, C. A. Isaza Rold√°n, F. Toapanta-Ramos, and A. Lobato-Campoverde. 2020. An√°lisis num√©rico de un sistema de calentamiento de agua utilizando un colector solar de placa plana. Ingenius. https://doi.org/10.17163/ings.n24.2020.10.
Rangababu, J. A., K. Kiran Kumar, and S. Srinivasa Rao. 2015. "Numerical Analysis and Validation of Heat Transfer Mechanism of Flat Plate Collectors." *Procedia Engineering* 127. https://doi.org/10.1016/j.proeng.2015.11.331.

Sami, S., E. Marin, and J. Rivera. 2016. "Numerical Analysis of Thermosyphon Solar Water Heaters." *International Journal of Energy and Power Engineering* 5 (2): 83. https://doi.org/10.11648/j.ijepe.20160502.18

Souliotis, M. 2021. *Flat Plate Solar Thermal Collector*. Mendeley Data.

Vetter, B., S. Fischer, and H. Dr√(ck. 2018. CFD-Based Development, Testing and Optimization of Flat Plate Collectors. https://doi.org/10.18086/eurosun2018.12.03.

Wang, N., S. Zeng, M. Zhou, and S. Wang. 2015. "Numerical Study of Flat Plate Solar Collector with Novel Heat Collecting Components." *International Communications in Heat and Mass Transfer* 69. https://doi.org/10.1016/j.icheatmasstransfer.2015.10.012.